THE JOURNAL OF PHYSICAL CHEMISTRY A
A JOURNAL OF THE AMERICAN CHEMICAL SOCIETY

pubs.acs.org/JPCA

Article

Role of Exact Exchange in Difference Projected Double-Hybrid Density Functional Theory for Treatment of Local, Charge Transfer, and Rydberg Excitations

Emily M. Kempfer-Robertson, Meagan N. Haase, Jonathan S. Bersson, Irma Avdic, and Lee M. Thompson*

Cite This: https://doi.org/10.1021/acs.jpca.2c04338

Read Online

ACCESS | Metrics & More | Article Recommendations | Supporting Information

ABSTRACT: Difference approaches to the study of excited states have undergone a renaissance in recent years, with the development of a plethora of algorithms for locating self-consistent field approximations to excited states. Density functional theory is likely to offer the best balance of cost and accuracy for difference approaches, and yet there has been little investigation of how the parametrization of density functional approximations affects performance. In this work, we aim to explore the role of the global Hartree−Fock exchange parameter in tuning accuracy of different excitation types within the framework of the recently introduced difference projected double-hybrid density functional theory approach and contrast the performance with conventional time-dependent double-hybrid density functional theory. Difference projected double-hybrid density functional theory was demonstrated to give vertical excitation energies with average error and standard deviation with respect to multireference perturbation theory comparable to more expensive linear-response coupled cluster approaches (*J. Chem. Phys.***2020**, *153*, 074103). However, despite benchmarking of local excitations, there has been no investigation of the methods performance for charge transfer or Rydberg excitations. In this work we report a new benchmark of charge transfer, Rydberg, and local excited state vertical excitation energies and examine how the exact Hartree−Fock exchange affects the benchmark performance to provide a deeper understanding of how projection and nonlocal correlation balance differing sources of error in the ground and excited states.

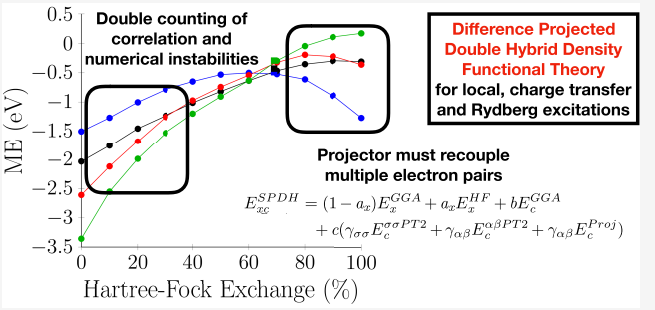

INTRODUCTION

The development of new light-based technologies requires accurate and computationally efficient excited state methodologies to model medium and large systems. Examples of important processes which require an atomistic understanding of different photochemical pathways include light-harvesting,[1,2] biological fluorescence,[3,4] and solar cells.[5−7] The most popular methodology for studying the excited states of large systems is time-dependent density functional theory (TDDFT), which provides a semiquantitative description of local excitations in the vertical excitation region.[8,9] Despite the utility of TDDFT, well-known issues include inabilities to describe charge-transfer states, double-excited states, Rydberg states, and electronic degeneracies with the ground state.[10−13] Numerous improvements to the TDDFT methodology have partially resolved some issues, including range separated functionals to describe charge transfer[14−16] and inclusion of select double-substituted determinants to describe conical intersections.[17] In addition, improved accuracy can be obtained using a double-hybrid TDDFT formalism[18−23] or within a wave function formalism using linear-response coupled cluster singles and approximate doubles (LR-CC2) or equation-of-motion coupled cluster singles and doubles (EOM-CCSD) approaches.[24,25]

Although double-hybrid (DH) approaches increase the computational scaling of TDDFT approaches to noniterative $O(N^5)$, they can often rival the accuracy of more expensive wave function-based approaches[26,27] while correcting TDDFT errors in systems such as singlet−singlet valence excitations in large organic dyes,[28,29] electronic circular dichroism spectra,[30] and excited states in polycyclic aromatic hydrocarbons.[31] Despite the successes of DH methods, they give an unsatisfactory description of charge transfer and Rydberg states,[32−35] which can be partially ameliorated through use of range separation.[14,36−39] However, the range separation parameter is system-dependent,[40] and although the exact

Received: June 22, 2022
Revised: October 8, 2022

exchange parameter has been investigated for ground state transition metal complexes,[41] there has yet to be a study of how exact exchange affects the accuracy of charge transfer, Rydberg, and local vertical excitation energies within a difference formalism.

In previous work, we have described an alternative double-hybrid DFT (DH-DFT) approach for modeling excited states which was found to give results of similar quality to LR-CC2 or EOM-CCSD despite the lower computational scaling.[27] The difference projected double-hybrid density functional theory (Δ-Proj-DH-DFT) method uses projection to resolve the imbalance in the description of dynamic and static correlation which diminishes the accurate calculation of vertical excitation energies. Furthermore, reoptimization of orbitals in difference methods for each electronic state accounts for orbital relaxation effects in response to electron transitions. The Δ-Proj-DH-DFT methodology requires self-consistent field (SCF) reference wave functions for each electronic state of interest. The orbitals of each SCF solution are optimized using density functional theory (DFT), where direct use of the unimproved SCF solutions defines the difference density functional theory (ΔDFT) approach. In the case where a double-hybrid functional is used in the SCF optimization, the resulting solutions give a difference double-hybrid density functional theory (ΔDH-DFT) approach. While ΔDH-DFT would be expected to recover a significant portion of the dynamic correlation, symmetry breaking and subsequent projection to restore symmetry can recover static correlation. Projection either can be performed during the variational procedure leading to a modified set of orbitals or can be performed after variation on the orbitals obtained without projection. When projection is applied to the DFT solutions, the method is known as difference projected density functional theory (Δ-Proj-DFT), while projection applied to the DH-DFT solutions is known as Δ-Proj-DH-DFT. It is relevant to note that DFT suffers from spin contamination to a lesser extent than Hartree−Fock (HF) wave functions, although for low-spin open shell systems, any single-reference methodology will eventually exhibit symmetry breaking.[42] In the context of excited electronic states, the breaking of an electron pair will always lead to large contributions from contaminating spin states, while the amount of HF exchange may modulate the extent of symmetry breaking in the remaining $N - 2$ electrons. Correlation generally reduces spin contamination (although not always[43]), although the presence of spin contamination is known to significantly impact the convergence of the Møller−Plesset perturbation series.[44,45]

Our previous studies focused only on local excitations and revealed surprisingly that Δ-Proj-DFT gave significantly worse performance than ΔDFT. As a result, in this work we examine a broader class of excitation types, including local, charge-transfer, and Rydberg states. We investigate how inclusion of exact exchange affects the relative performance of Δ-Proj-DH-DFT and underlying methodologies. The goal of this study is to provide a systematic understanding of how the exact exchange parameter can be tuned for different excitation types, as well as establish if the previous failures of ΔDFT are a result of the functional parametrization. In the remainder of the article, we first discuss the overall performance of Δ-Proj-DH-DFT on three types of vertical excitation energies (local, charge transfer, and Rydberg excitations) and compare the results with conventional time-dependent double-hybrid density functional theory (TDDHDFT). The local excitations tested are a different set to those used in our previous work, so our goal is to ensure our previous findings are transferrable as well as provide additional data on the models performance. As our previous work found insignificant difference between functionals, we only use the DSDPBEP86 functional throughout this study. Second, we examine the role of the HF exchange contribution for improving the description of difference vertical excitation energies (VEEs), particularly for Rydberg and charge transfer excitations which from linear-response TDDFT are known to require nonlocal exchange to correct for self-interaction error and describe the long-range component of the exchange−correlation hole. Lastly, we conclude by describing the successes, limitations, and future directions of the Δ-Proj-DH-DFT methodology.

METHODS

Construction of Projection Operators. The Δ-Proj-DH-DFT method[27] uses projection to recover correlation energy from a symmetry broken Kohn−Sham (KS) determinant. Although Δ-Proj-DH-DFT uses a KS determinant, the formulation is analogous to methods constructed from a HF determinant, and so in this section, we describe in general terms the construction of projection operators in the context of the wave function. Further modifications for projection of KS based methods are then developed in the following section. Projectors can be used to recover good quantum numbers from symmetry-broken approximate wave functions $|\Phi_0\rangle$ by removing terms with incorrect S and M_S quantum numbers resulting from spin contamination. Generally, any wave function (including post-SCF) can be written in terms of the contributions from eigenfunctions with different S and M_S quantum numbers

$$|\Phi_0\rangle = \sum_S \sum_{M_S} c_{S,M_S} |S, M_S\rangle \tag{1}$$

where c_{S,M_S} are expansion coefficients. For spin-adapted wave functions, all but one of the c_{S,M_S} are zero, while for wave functions that have spin polarization (collinear and noncollinear), only c_{S,M_S} with the same M_S are nonzero. In the case that electron spins are not confined along a common spin axis (coplanar or noncoplanar), all c_{S,M_S} may be nonzero. If only the component of the wave function with spin quantum numbers S' and M_S' is desired, undesired components can be removed by acting on the wave function with the projector $\hat{P}_{S',M_S'}$

$$\begin{aligned} |S', M_S'\rangle &= \hat{P}_{S',M_S'} |\Phi_0\rangle \\ &= \mathcal{N} \sum_S \sum_{M_S} c_{S,M_S} |S', M_S'\rangle \langle S', M_S' | S, M_S\rangle \end{aligned} \tag{2}$$

where $\mathcal{N}$ normalizes the wave function, and due to the orthonormality of spin eigenfunctions,

$$\langle S', M_S' | S, M_S\rangle = \delta_{SS'} \delta_{M_S M_S'}$$

thus selecting only the desired spin component of the wave function. In the remainder of this text we deal only with projection of collinear SCF solutions. One approach to realize the projection expressed in eq 2 is to diagonalize the Hamiltonian built from a determinant expansion in the space of biorthogonal orbital pairs which have nonunit overlap. The eigenvectors then provide the coefficients that indicate how each spin-adapted eigenfunction of the Hamiltonian contrib-

https://doi.org/10.1021/acs.jpca.2c04338
J. Phys. Chem. A XXXX, XXX, XXX−XXX

utes to the symmetry-broken wave function. The projected energy E^P can then be obtained from

$$E^P = \frac{\sum_{I\in\langle\hat{S}^2\rangle=S_z(S_z+1)} c_I^* c_I E_I}{\sum_{I\in\langle\hat{S}^2\rangle=S_z(S_z+1)} c_I^* c_I} \tag{3}$$

where the summations only include pure-spin states of the desired $\langle\hat{S}^2\rangle$ value and the denominator normalizes the wave function. While the formalism of eq 3 is useful for conceptually understanding how projection works, the factorial scaling of the size of the determinant expansion in terms of the number of biorthogonal orbital pairs with nonunitary overlap undermines its practical utility.

Instead of explicitly constructing and diagonalizing the Hamiltonian in the basis of the biorthogonal determinant expansion, Löwdin proposed a projector that, while not resolving the factorial scaling required to fully project the wave function, can be used to project only the spin states that most contaminate the wave function[46]

$$\hat{P}_S = \prod_{K=S+1}^{1/2(N_\alpha+N_\beta)} \frac{\hat{S}^2 - K(K+1)}{S(S+1) - K(K+1)} \tag{4}$$

where for collinear systems with spin aligned on the z axis $S = S_z = \frac{1}{2}(N_\alpha - N_\beta)$, i.e., the total electron spin projected along the axis of spin quantization, and N_α and N_β are the number of α and β electrons, respectively. In the case of single excitations where a single electron pair is broken, the $S + 1$ spin state contaminates to a far greater extent than any other. As a result, the projector in eq 4 can be truncated at $K = S + 1$ and the resulting projector is known as the annihilation operator

$$\hat{A}_{S+1} = \frac{\hat{S}^2 - (S+1)(S+2)}{S(S+1) - (S+1)(S+2)} \tag{5}$$

Alternatively, the Wheeler−Hill coordinate generator formulation[47,48] leads to a projector that ensures invariance of the wave function with respect to the axis of spin quantization

$$\hat{P}_S = \frac{2S+1}{2}\int_0^\pi d\beta\, \sin(\beta) d^S_{M_S M_S}(\beta) e^{i\beta\hat{S}_y} \tag{6}$$

where $d^S_{M_S M_S}(\beta)$ is the Wigner small d matrix and $e^{i\beta\hat{S}_y}$ is the collective rotation of the angle of spin quantization by an angle β. The advantage of the approach in eq 6 is that projection of all contaminating spin states is possible at mean-field cost and so resolves the factorial scaling or truncation of the Löwdin projector.

Projection-after-Variation Double-Hybrid Density Functional Theory. In the Δ-Proj-DH-DFT approach, the ground and excited states are computed by local optimization of two SCF solutions representing each state of interest which are generally symmetry broken. For the excited state, breaking an orbital pair always results in spin contamination at the SCF level that requires projection to resolve, while low spin open shell electronic structure in the ground state will also require projection. In the current implementation, the projector of eq 5 is used to provide a corrected energy using

$$E^P = \frac{\langle\Phi_0|\hat{H}\hat{A}_{S+1}|\Phi_0\rangle}{\langle\Phi_0|\hat{A}_{S+1}|\Phi_0\rangle} \tag{7}$$

where, as above, the exact nature of $|\Phi_0\rangle$ depends upon the specific methodology being used. The projector in eq 5 is strictly valid only when one electron spin-pair is broken in the excitation and when the remaining orbitals are closed shell in both the ground and excited state. However, our previous work indicated that severe degradation of VEEs does not occur until $\langle\hat{S}^2\rangle$ closely approaches $(S + 1)(S + 2)$, which is indicated by an increase in $\langle\hat{S}^2\rangle$ upon annihilation. An additional source of error is the inability of symmetry breaking and projection to describe more than a single correlation mechanism, in which natural orbitals from several different symmetry-broken SCF solutions are required to capture the static correlation.[49,50]

In the case where $|\Phi_0\rangle$ is a HF or KS determinant, inserting eq 5 into eq 7 yields the projected SCF energy E^{PSCF}

$$E^{PSCF} = \langle\Phi_0|\hat{H}|\Phi_0 + \tilde{\Phi}_1\rangle \tag{8}$$

where

$$|\tilde{\Phi}_1\rangle = \sum_{ijab} \frac{|\Phi_{ij}^{ab}\rangle\langle\Phi_{ij}^{ab}|\hat{S}^2|\Phi_0\rangle}{\langle\hat{S}^2\rangle - (S+1)(S+2)} \tag{9}$$

is the correction to the SCF solution, in which $|\Phi_{ij}^{ab}\rangle$ are determinants obtained from double substitution of electrons with respect to $|\Phi_0\rangle$, with indices $i, j, k, \ldots$ referring to occupied orbitals and $a, b, c, \ldots$ referring to virtual orbitals. In the case of second-order Møller−Plesset perturbation theory (MP2), the projected energy E^{PMP2} is

$$E^{PMP2} = \langle\Phi_0|\hat{H}|\Phi_0 + \Phi_1 + \tilde{\Phi}_1'\rangle \tag{10}$$

where $|\tilde{\Phi}_1'\rangle$ is obtained by Gram−Schmidt orthogonalization of the first order correction

$$|\Phi_1\rangle = -\sum_{ijab} \frac{|\Phi_{ij}^{ab}\rangle\langle\Phi_{ij}^{ab}|\hat{H}|\Phi_0\rangle}{\Delta_{ijab}} \tag{11}$$

where ε is the orbital energy and $\Delta_{ijab} = \varepsilon_a + \varepsilon_b - \varepsilon_i - \varepsilon_j$, with $|\tilde{\Phi}_1\rangle$, yielding

$$|\tilde{\Phi}_1'\rangle = |\tilde{\Phi}_1\rangle \left(1 + \frac{\sum_{ijab}\langle\Phi_0|\hat{S}^2|\Phi_{ij}^{ab}\rangle t_{ij}^{ab}\{\langle\hat{S}^2\rangle - (S+1)(S+2)\}}{\sum_{ijab}|\langle\Phi_0|\hat{S}^2|\Phi_{ij}^{ab}\rangle|^2}\right) \tag{12}$$

where t_{ij}^{ab} are the MP2 amplitudes

$$t_{ij}^{ab} = \frac{\langle ij\|ab\rangle}{\Delta_{ijab}} \tag{13}$$

Owing to the singularities in t_{ij}^{ab} due to the small orbital energy gaps in the denominator, which is particularly acute when performing MP2 corrections to excited states (and with low amounts of exact exchange in the case of DH-DFT), we have further investigated the use of regularized amplitudes $\tilde{t}_{ij}^{ab}$[51]

$$\tilde{t}_{ij}^{ab} = t_{ij}^{ab}(1 - \exp\{-\lambda\Delta_{ijab}\})^2 \tag{14}$$

which goes to zero as $\Delta_{ijab} \to 0$ and where λ is a parameter that controls the regularization strength. The regularized ampli-

https://doi.org/10.1021/acs.jpca.2c04338
J. Phys. Chem. A XXXX, XXX, XXX−XXX

tudes are used in both $|\Phi_1\rangle$ and $|\tilde{\Phi}_1'\rangle$ components of the DH-DFT functional.

Using a double-hybrid Kohn−Sham density in eq 10, the projected double-hybrid density functional theory (PDH-DFT) energy can be written as

$$E^{PDH} = \langle \Phi_0 | \hat{H} | \Phi_0 + \gamma(\Phi_1 + \tilde{\Phi}_1') \rangle \quad (15)$$

where γ is the parameter than governs the amount of MP2 correlation in the double-hybrid functional. The exchange−correlation components of eq 15 can be written as

$$E_{xc}^{PDH} = (1 - a_x)E_x^{GGA} + a_x E_x^{HF} + bE_c^{GGA} + c(\gamma_{\sigma\sigma}E_c^{\sigma\sigma PT2} + \gamma_{\alpha\beta}E_c^{\alpha\beta PT2} + \gamma_{\alpha\beta}E_c^{Proj}) \quad (16)$$

where the first three terms are standard exchange and correlation terms from hybrid DFT, the fourth and fifth terms are the MP2 correlation terms, which can be broken into same-spin ($\sigma\sigma$) and opposite-spin ($\alpha\beta$) components, and the final term is the projection contribution accounting for symmetry breaking in the reference Kohn−Sham orbitals. The coefficients a_x, b, c, and γ are free parameters which can be fitted to a training set. An advantage of projection is that it does not increase the number of empirical parameters in the functional. As a result, in our previous work, we were able to examine the use of three functionals (PBEQIDH, B2PLYP, and DSDPBEP86), along with MP2, without having to determine a suitable parameter for the projection term. Although a significant improvement was found upon use of a Kohn−Sham reference, there was no significant difference in the performance of different functionals. However, all functionals tested used a large amount of HF exchange, with a_x between 0.53 and 0.69, which raised the question about whether the apparent failure of Δ-Proj-DFT observed in our previous study resulted from a combination of suboptimal parameters. In addition, high HF exchange character leads to greater symmetry breaking of the reference and so may overemphasize the importance of projection.

Computational Details. In order to ascertain the role of HF exchange on the accuracy of Δ-Proj-DH-DFT calculations, we first examined the performance using the benchmark set of Tozer et al.[52] The benchmark set consists of 32 local excitations, 14 charge transfer excitations, and 13 Rydberg excitations. Owing to the similarity in the performance of different functionals previously observed, only DSDPBEP86 was used, as spin-component scaled terms have been implicated in separating the parametrization of long-range (same-spin) and short-range (opposite-spin) interactions important for a balanced description of correlation energy change upon excitations.[53−55] The basis sets used were cc-pVTZ for dipeptide, β-dipeptide, tripeptide, *N*-phenylpyrrole (PP), 4-(*N*,*N*-dimethylamino)benzonitrile (DMABN) and HCl; and d-Aug-cc-pVTZ for N_2, CO, and H_2CO. The use of diffuse functions when studying N_2, CO, and H_2CO was due to the Rydberg character of the excited electronic states. Ground states were determined by computing the lowest energy real restricted solution and then performing analysis of the orbital-rotation Hessian to ensure no instabilities with respect to occupied-virtual (ov) rotations were present. All molecules were found to have stable restricted SCF solutions in the ground state. Excited states were obtained by swapping relevant ov orbital pairs in the real-restricted determinant and then optimizing using the maximum overlap method (MOM)[56,57] or state-targeted energy projection (STEP)[58] with real-unrestricted symmetry. A more detailed description of the workflow required to determine the SCF solutions corresponding to both ground and excited states is outlined in section 7 of the Supporting Information. Both ground and excited state energies were calculated using the reference functional (PBEP86), the projected reference functional (projected PBEP86), the double-hybrid functional (DSDPBEP86), and the projected double-hybrid functional (projected DSDPBEP86). To ascertain the role of HF exchange, the value of a_x in eq 16 was varied in increments of 0.1 from zero to one. Vertical excitation energies were also computed using TD-DSDPBEP86 in order to compare the performance of linear response and difference DH-DFT. All calculations were performed using a modified version of Gaussian 16,[59] other than TDDHDFT calculations which used Orca,[60] and the Wheeler−Hill coordinate generator projection method which was implemented in a stand-alone code using the MQCPack library[61] interfaced with Gaussian. Difference vertical excitations energies were compared to benchmark reference values determined in ref 52 from gas-phase experimental data, state specific complete active space with second order perturbation theory (CASPT2), and LR-CC2 computational data.

RESULTS AND DISCUSSION

This section details the performance of Δ-Proj-DH-DFT for calculated local, charge transfer, and Rydberg VEEs. First, we discuss the performance of Δ-Proj-DH-DFT VEEs for different excitation types using original parametrization for the ground state (69% HF exchange) used in our original study and compare the result with state-of-the-art conventional TDDHDFT. We then discuss how the performance of Δ-Proj-DH-DFT VEEs changes depending on the percentage of HF exchange. Our analysis breaks the performance down into local, charge transfer, and Rydberg excitations, as well as overall performance.

DSDPBEP86 Vertical Excitation Energies Using Original Parametrization. The standard deviations and mean errors of difference unprojected and projected hybrid and double-hybrid functionals for computing VEEs of local, charge transfer, and Rydberg states using the original parametrization (69% HF exchange) are shown in Table 1. We first comment on the performance of the local excitations in the Tozer benchmark set (ref 52) and contrast the results with our previous study, in which the Thiel benchmark set (ref 62) consisting of only local excitations was used. Subsequently, we examine the results of difference unprojected and projected functionals for computing charge transfer and Rydberg states, which have not previously been explored using difference methods. Results using a difference formalism are compared to TDDHDFT results with the same functional.

The results shown in column 3 of Table 1, which detail the local excitations of the Tozer benchmark, are broadly in agreement with the results using the Thiel benchmark in column 6, with decreasing mean error and standard deviation with the number of terms in the functional.[27] In terms of standard deviations, all methods gave slightly better results in the Tozer benchmark than the Thiel benchmark, improving by 0.09−0.26 eV depending on the number of terms included in the functional. ΔDFT gave the largest improvement in standard deviation between benchmarks by 0.26 eV, although it still performed worse than either of the two MP2 corrected

https://doi.org/10.1021/acs.jpca.2c04338
J. Phys. Chem. A XXXX, XXX, XXX−XXX

Table 1. Mean Error (ME), Mean Absolute Error (MAE), and Standard Deviation (SD) in eV for Vertical Excitation Energies to Local, Charge Transfer, and Rydberg Electronic States Compared to Benchmark Values in Refs 52 and 62, Computed Using Δ-Proj-DSDPBEP86 and Underlying Methods

		type of excitation			
		this work (Tozer)			ref 27 (Thiel)
method/functional		local	charge transfer	Rydberg	local
Δ-Proj-DSDPBEP86	ME	−0.19	−0.66	−0.16	−0.29
	MAE	0.37	0.75	0.51	0.58
	SD	0.44	0.57	0.61	0.53
Δ-DSDPBEP86	ME	−0.31	−0.31	−0.24	−0.40
	MAE	0.47	0.52	0.33	1.09
	SD	0.53	0.44	0.37	0.66
Δ-Proj-PBEP86[a]	ME	−0.35	−1.02	−0.27	−0.04
	MAE	0.82	1.12	1.14	0.69
	SD	1.07	0.67	1.37	1.15
Δ-PBEP86[a]	ME	−0.50	−0.35	−0.35	−0.17
	MAE	0.67	0.47	0.53	0.94
	SD	0.61	0.46	0.60	0.86

[a]Methods use nonstandard 69% exact exchange.

Table 2. Mean Error (ME), Mean Absolute Error (MAE), and Standard Deviation (SD) in eV for Vertical Excitation Energies to Local, Charge Transfer, and Rydberg Electronic States Compared to Benchmark Values in Ref 52, Computed Using Time-Dependent Density Functional Theory with Different Functionals

		type of excitation		
method/functional		local	charge transfer	Rydberg
TD-DSDPBEP86	ME	−0.19	−1.52	−0.21
	MAE	0.38	1.68	0.49
	SD	0.43	1.42	0.54
TD-CAM-B3LYP[a]	ME	0.02	−0.81	−0.50
	MAE	0.20	0.27	0.50
	SD	0.27	0.31	0.18
TD-B3LYP[a]	ME	−0.15	−1.35	−1.11
	MAE	0.22	1.36	1.11
	SD	0.26	0.86	0.23
TD-PBE[a]	ME	−0.31	−2.60	−1.84
	MAE	0.33	2.60	1.84
	SD	0.27	1.37	0.30

[a]Results from ref 52.

methods. As was observed in the Thiel test set, the Tozer test set also revealed Δ-Proj-DFT gave a worse standard deviation than the unprojected ΔDFT, indicating that without MP2 correlation, projection should not be used with ΔDFT results. In terms of mean error, the Tozer benchmark corroborated the findings using the Thiel benchmark that difference methods systematically underestimate VEEs. MP2 corrected methods give improved mean errors in the Tozer benchmark, while the reference functionals give worse mean errors. As a result, the Tozer benchmark gives the expected order of improvement in mean error with the number of terms in the functional. The fact that functionals without MP2 correlation give worse results is likely a result of the larger standard deviation so that the anomalously low mean error of Δ-Proj-DFT in the Thiel benchmark (−0.04 eV) was a consequence of sign cancellation. Despite the fact that both the Tozer and the Thiel benchmark sets showed projection increased the standard deviation of ΔDFT, both benchmarks showed projection reduced the mean error, even though the mean error of Δ-Proj-DFT was inconsistent between benchmarks. In comparison to the TDDFT results (Table 2), the DFT difference methods result in larger standard deviations than those obtained using TDDFT except for TD-DSDPBEP86, which surprisingly had greater standard deviation that any of the lower-rung density functionals (TD-PBE standard deviation is 0.27 eV, TD-B3LYP is 0.26 eV, TD-CAM-B3LYP is 0.27 eV, and TD-DSDPBEP86 is 0.43 eV). The performance of TDDHDFT in terms of standard deviation was almost identical to Δ-Proj-DH-DFT and yet better than unprojected ΔDH-DFT. While the mean error of ΔDFT is larger than any of the functionals tested using TDDFT, Δ-Proj-DFT and ΔDH-DFT give similar mean errors to TD-PBE (−0.31 eV), while Δ-Proj-DH-DFT gives a mean error similar to TD-B3LYP (−0.15 eV) and TD-DSDPBEP86 (−0.19 eV) for local excitations. The competitiveness of TDDFT with difference methods is perhaps unsurprising as TDDFT is known to perform well for local excitations.

We now turn to discuss the Rydberg and charge transfer excitations which were not included in the Thiel benchmark set, and so it is not possible to evaluate results from the Tozer benchmark in the context of previous results. A key finding of ref 52 is that additional HF exchange improves the performance of all excitations in linear-response TDDFT, particularly for Rydberg and charge transfer states, and so the high HF exchange of double-hybrid functionals is likely to give good performance in difference methods. All difference methods (Table 1, column 4) give results for charge transfer excitations that are better than TD-PBE, TD-B3LYP, and TD-DSDPBEP86 in terms of both mean error and standard deviation. Only unprojected methods (with or without the MP2 correction) are able to approach the standard deviation of TD-CAM-B3LYP, although TD-CAM-B3LYP has a much larger mean error. The standard deviations and mean errors of charge transfer states show unprojected methods give better results than projected methods, regardless of whether MP2 correlation is included in the functional. Using difference methods to compute VEEs of Rydberg states, all methods gave better mean errors than TD-CAM-B3LYP or TD-DSDPBEP86, with the number of terms in the functional correlating with a decrease in the mean error. However, difference methods gave a larger standard deviation than linear-response approaches, with projection diminishing the performance of hybrid and double-hybrid functionals. Based on these findings, while projection improves the performance of difference methods for studying local excitations, for charge transfer and Rydberg excitations, the use of projection can lead to reduced accuracy and/or precision. As a result, we seek to understand the origin of the failure of projection when applied to Rydberg and charge transfer states and whether the performance can be improved by alternative parametrizations.

Effect of Exact Exchange Parameter on Δ-Proj-DH-DFT Vertical Excitation Energies. In this section, we seek to establish the role of the value of a_x in tuning the performance

https://doi.org/10.1021/acs.jpca.2c04338
J. Phys. Chem. A XXXX, XXX, XXX−XXX

of ΔDH-DFT methods for local, charge transfer, and Rydberg excitations.

Local Excitations. The mean error and standard deviation of local excitation VEEs as a function of HF exchange percentage are shown in Figure 1, with numerical values

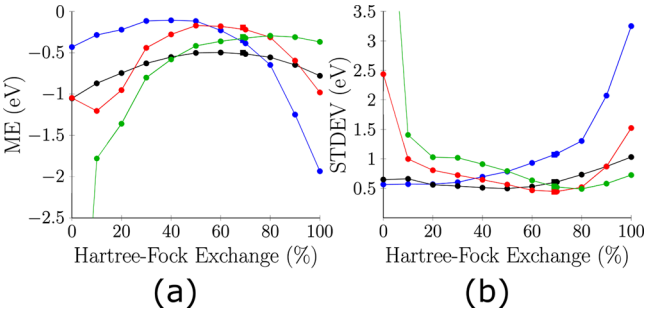

Figure 1. Mean error (a) and standard deviation (b) of local excitation vertical excitation energies as a function of Hartree−Fock exchange percentage for ΔPAV-DH-DFT (red), ΔDH-DFT (green), ΔPAV-DFT (blue), and ΔDFT (black) compared to benchmark values. Squares show the results at 69% Hartree−Fock exchange.

provided in Table S7. The results in Table 1, with the original HF exchange parameter, are indicated by squares, while circles indicate results with differing values of HF exchange ranging between 0% and 100%. The mean error of Δ-Proj-DH-DFT, shown in Figure 1a (red), does not change significantly between 40% and 80%, with values between −0.31 eV and −0.17 eV. At 60% and 70% Δ-Proj-DH-DFT is the best performing functional in terms of mean error, although the smallest Δ-Proj-DH-DFT mean error is actually obtained at 50% HF exchange (−0.17 eV). Therefore, the standard HF exchange value of most double-hybrid functionals, which typically lie between 50% and 70%, is likely to be a reasonable choice for calculating local VEEs. At low amounts of HF exchange, both projected and unprojected double-hybrid methods rapidly degrade in performance and the hybrid functionals become the best performing methods. Δ-Proj-DFT (blue) is the best performing method at 50% HF exchange and below. In fact, the global minimum mean error in terms of functional and HF exchange percentage is Δ-Proj-DFT with 40% HF exchange, which gives a value of −0.11 eV. At 20% HF exchange, Δ-Proj-DFT is competitive with the best performing double-hybrid parametrization in terms of both mean error and standard deviation. However, as will be demonstrated below and is observed in TDDFT, the performance of hybrid functionals is not transferable to charge transfer and Rydberg VEEs.

The reason the double hybrids systematically fail with low HF exchange contributions is a result of double counting static correlation through both the DFT exchange and MP2 correlation parts, which has previously been highlighted by Grimme.[63] Additionally, recent findings by Santra and co-workers have indicated that double-hybrid functionals parametrized with lower HF exchange, which results in a smaller frontier orbital energy gap,[64] may benefit from regularization,[65] indicating that the reduced performance of double-hybrids with low HF exchange is also in-part due to the numerical consequences of the smaller orbital energy gap. The effect of the HOMO−LUMO energy gap on the relative performance of hybrid and double hybrid functionals is illustrated in Figure 2 for all excitation types, while Figures S3, S4, and S5 show the

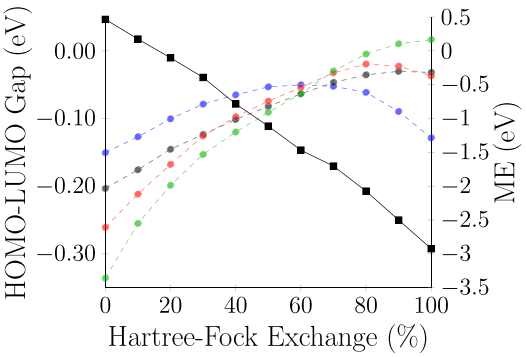

Figure 2. Role of exact exchange in controlling the average excited state HOMO−LUMO energy difference (black squares, left axis) and the correlation between mean error (right axis) in ΔPAV-DH-DFT (red), ΔDH-DFT (green), ΔPAV-DFT (blue), and ΔDFT (black). Graph shows results for all excitation types (local, charge transfer, and Rydberg).

same trend broken down by excitation type. At low amounts of HF exchange the average frontier orbital energy gap rapidly approaches zero (black line, left axis), resulting in the mean error of both projected and unprojected double hybrid functionals (green and red lines, respectively, right axis) increasing to a greater extent than either unprojected or projected hybrid functionals (black and blue respectively). Using regularization at low amounts of exact exchange, in which eq 14 is employed with $\lambda = 1.45$, changes the mean error of Δ-Proj-DH-DFT to −0.41 eV from −1.05 eV, suggesting the presence of small HOMO−LUMO gaps has an effect on the methods performance.

At high amounts of HF exchange, the projected methods drop off in performance, whether the projection is performed on the hybrid or double-hybrid functional. At 80% HF exchange and above, the unprojected ΔDH-DFT becomes the best performing methodology, while at the same HF exchange value, ΔDFT overtakes Δ-Proj-DFT in performance. One reason for the failure of projection at high HF exchange values is due to the fact that symmetry breaking is greater when more HF exchange is included, potentially causing the Löwdin annihilator to fail when spin polarization of electron pairs that are not involved in the excitation occurs. When the analysis is performed excluding states where the $\langle \hat{S}^2 \rangle$ increases upon annihilation (Figure S1), the projected methods are found to improve slightly but not change the qualitative results when including these ill-behaved states. The robustness of the Löwdin annihilation operator to multiple spin contaminants in both the Thiel and the Tozer benchmarks is somewhat surprising, as it is known to lead to completely incorrect behavior in the dissociation of linear H_4.[66] However, while annihilation of the $(S_z + 1)$ contaminating state that leads to an increase in $\langle \hat{S}^2 \rangle$ is a clear indicator of failure of the projection, it is also possible that even in cases where projection $\langle \hat{S}^2 \rangle$ does not increase, the contamination of unprojected higher-order spin multiplicities may still adversely affect performance. As demonstrated below for charge-transfer excitations, higher order contamination can still pay a significant role even in cases where $\langle \hat{S}^2 \rangle$ does not increase upon annihilating the $(S + 1)$ contaminating state. As a result, the reduced performance of the projected methods at high HF exchange is a consequence

https://doi.org/10.1021/acs.jpca.2c04338
J. Phys. Chem. A XXXX, XXX, XXX−XXX

of the limitations of the particular form of the projector used rather than projection generally.

The trend in standard deviation (Figure 1b) follows almost exactly the same trends as the mean error, with MP2 correlation corrected functionals performing worse at low HF exchange percentage and projected functionals performing worse at high HF exchange percentages. All four methods are, at some HF exchange percentage, the best performing method in terms of standard deviation. Interestingly, despite being the better performing method in terms of mean error, Δ-Proj-DFT has significantly worse standard deviation than ΔDFT at all but low HF exchange percentages. The lowest standard deviation of Δ-Proj-DH-DFT is achieved when the HF exchange is at 69%, indicating the default parameters are the most suitable for calculating VEEs of local excitations. As a result, the combination of low mean error and standard deviation indicates that Δ-Proj-DH-DFT is the functional that will deliver the most accurate and precise results.

Charge Transfer Excitations. In this section we discuss the performance of Δ-Proj-DH-DFT in describing charge transfer excitations as a function of HF exchange (Figure 3). In terms

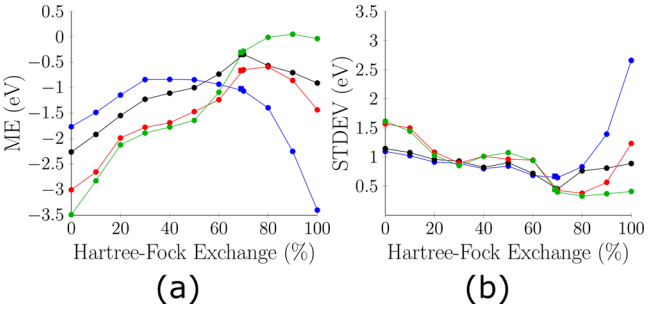

Figure 3. Mean error (a) and standard deviation (b) of charge transfer vertical excitation energies as a function of Hartree−Fock exchange percentage for ΔPAV-DH-DFT (red), ΔDH-DFT (green), ΔPAV-DFT (blue), and ΔDFT (black) compared to benchmark values. Squares show the results at 69% Hartree−Fock exchange.

of mean error, the best performing functional is unprojected ΔDH-DFT (green) at 80% exact exchange, which gives a value of −0.01 eV (Figure 3a). The mean error of unprojected ΔDH-DFT does not change significantly from 80 to 100% HF exchange, and in fact at 90% the VEEs are slightly overestimated in contrast to the general trend which underestimates VEEs. At low HF exchange values, the poor performance of MP2 corrected methods that was apparent in the local excitations is also present in charge transfer excitations, causing the hybrid functionals to become the better performing functionals between 0% and 60% HF exchange. Below 60% HF exchange, projection improves the VEE of charge transfer excitations, while at 60% HF exchange and above, projection gives worse performance as was also observed for local excitations. While the performance of Δ-Proj-DFT (blue) diminishes rapidly at 60% exact exchange and above, Δ-Proj-DH-DFT (red) reaches a minimum mean error of −0.59 eV at 80% HF exchange before performance diminishes. At around 70% HF exchange, the performance of hybrid and double-hybrid functionals cross so that at 69% HF exchange (squares) used in the standard parametrization, ΔDH-DFT gives a slightly smaller mean error than ΔDFT.

In terms of standard deviation (Figure 3b), projection does not result in a significant change in performance below 70% HF exchange. Above 70% HF exchange, the projected hybrid functional (blue) standard deviation rapidly deteriorates, while the projected double-hybrid (red) performance is slightly worse than the unprojected functionals. For both projected and unprojected double-hybrid functionals, the standard deviation is minimized with 80% HF exchange, while for hybrid functionals, the best standard deviation is at 70%. As for local excitations, diminished performance of projection methods at high HF exchange is partly due to the limitations of the Löwdin annihilation operator used as a projector in this work. In order to establish the extent to which the projector choice affects the functional performance, the analysis was recomputed excluding excitations to states in which $\langle \hat{S}^2 \rangle$ increased upon projection (Figure 4). At 70% HF exchange,

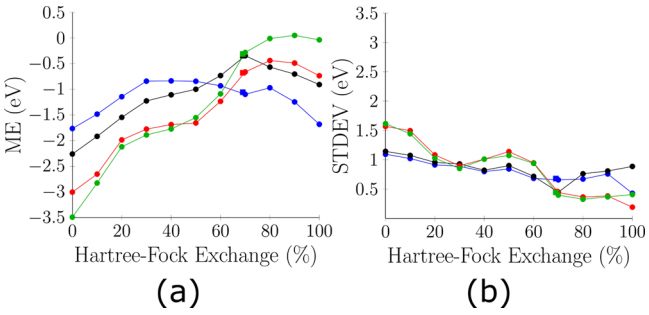

Figure 4. Mean error (a) and standard deviation (b) of charge transfer vertical excitation energies as a function of Hartree−Fock exchange percentage for ΔPAV-DH-DFT (red), ΔDH-DFT (green), ΔPAV-DFT (blue), and ΔDFT (black) compared to benchmark values, without data in which $\langle \hat{S}^2 \rangle$ of the reference increases upon projection. Squares show the results at 69% Hartree−Fock exchange.

one data point was removed, at 80%, five data points were removed, while at 90% seven data points were removed, and at 100% eight data points were removed. As shown in Figure 4a, both the projected hybrid and double-hybrid mean error and standard deviation improve at 70−100% once the anomalous data points are removed. However, even removing the anomalous data points, projection still resulted in larger mean error at high HF exchange.

To further assess if the increased mean error upon projection at high exact exchange is a result of higher-order contaminating states that cannot be projected by the Löwdin annihilator, even when the value of $\langle \hat{S}^2 \rangle$ does not increase upon projection, Table 3 shows the energy change as a result of increasing numbers of projected spin states on the unrestricted Hartree−Fock charge-transfer excited state energy. It is expected that, as higher spin states generally contribute less to contamination of symmetry-broken states, the energy change should decrease with each term in eq 4 as higher spin states are projected, i.e., the magnitude of the values should decrease across the row from column 3 to column 6 of Table 3. Indicated in the final column of Table 3 is the percentage exact exchange at which the excited PBE calculation showed an increase in the value of $\langle \hat{S}^2 \rangle$ upon annihilation of the triplet state. It is expected that states for which $\langle \hat{S}^2 \rangle$ increases at some amount of exact exchange would show larger energy changes when higher spin states are projected, than states for which $\langle \hat{S}^2 \rangle$ never increases upon projection. Analyzing Table 3, it can be seen that states for

https://doi.org/10.1021/acs.jpca.2c04338
J. Phys. Chem. A XXXX, XXX, XXX−XXX

Table 3. Change in the Difference Projected Hartree−Fock Vertical Excitation Energy of Charge Transfer Excitations as a Function of Number of Annihilated Spin States in kcal mol^{-1} [a]

		energy change on annihilation of indicated spin states (kcal mol^{-1})				
molecule	excitation	$\Delta E_{\mathrm{UHF}}^{\hat{A}(S+1)}$	$\Delta E_{\hat{A}(S+1)}^{\hat{A}(S+1,S+2)}$	$\Delta E_{\hat{A}(S+1,S+2)}^{\hat{A}(S+1,S+2,S+3)}$	$\Delta E_{\hat{A}(S+1,S+2,S+3)}^{\hat{A}(S+1\ldots S+\infty)}$	% exact exchange at which excited state PBE $\langle\hat{S}^2\rangle$ increases
dipeptide	$n_1 \rightarrow \pi_2^*$	−14.66	10.23	−0.18	−0.39	
	$\pi_1 \rightarrow \pi_2^*$	−57.31	45.30	−2.56	−0.13	80, 90, 100
β-dipeptide	$n_1 \rightarrow \pi_2^*$	−15.12	10.53	−0.18	−0.09	
	$\pi_1 \rightarrow \pi_2^*$	−62.12	49.48	−3.12	−0.13	90, 100
PP	$2\ ^1B_2$	−12.84	19.86	−1.05	−0.06	90, 100
	$3\ ^1A_1$	−45.42	37.25	−3.43	−0.06	80, 90, 100
DMABN	^1A	−51.74	56.77	−7.31	0.18	70, 80, 90, 100
HCL	$^1\Pi$	−2.67	6.70	−0.04	−0.04	
tripeptide	$\pi_1 \rightarrow \pi_2^*$	−9.85	16.77	−0.76	−0.07	100
	$\pi_2 \rightarrow \pi_3^*$	−57.48	45.56	−2.72	−0.13	80, 90, 100
	$\pi_1 \rightarrow \pi_3^*$	−66.01	52.72	−3.37	−0.13	80, 90, 100
	$n_1 \rightarrow \pi_3^*$	−16.41	11.31	−0.19	−0.08	
	$n_2 \rightarrow \pi_3^*$	−16.23	11.30	−0.21	−0.06	
	$n_1 \rightarrow \pi_2^*$	−16.59	11.55	−0.22	−0.53	

[a]The final column shows the exact exchange percentages at which $\langle\hat{S}^2\rangle$ of the excited state PBE calculation increased upon triplet annihilation $\hat{A}(S+1)$.

which $\langle\hat{S}^2\rangle$ increased for some amount of Hartree−Fock exchange in the projected DFT calculations displayed greater energy change upon projection of any contaminating spin state than states for which $\langle\hat{S}^2\rangle$ always decreased. For example, $\langle\hat{S}^2\rangle$ always decreases upon triplet annihilation of the dipeptide $n_1 \rightarrow \pi_2^*$ state, which shows smaller energy change upon projection than in the $\pi_1 \rightarrow \pi_2$ state, for which $\langle\hat{S}^2\rangle$ increases at 80% and above. However, even for states where $\langle\hat{S}^2\rangle$ decreases regardless of the amount of exact exchange, the energy change upon annihilation of the $(S+2)$ contaminating state (Table 3, column 4) is comparable to the energy change upon annihilation of the $(S+1)$ contaminating state (Table 3, column 3). Using the dipeptide $n_1 \rightarrow \pi_2^*$ as an example again, annihilation of the $(S+1)$ state changes the energy by −14.66 kcal mol^{-1}, while further projecting the $(S+2)$ state increases the energy by 10.23 kcal mol^{-1} over the $(S+1)$ annihilated state. The large energy changes upon annihilation of both $(S+1)$ and $(S+2)$ demonstrate the large role these two states play in the contamination of the charge transfer excited states. Annihilation of the $(S+3)$ state (Table 3, column 5) has little effect on the energy for all but the most contaminated charge transfer states, e.g., DMABN, while full projection reveals that contamination beyond the $(S+3)$ state is small for all states (Table 3, column 6). Although it is not possible to directly compare the results in Table 3 which use a symmetry broken HF determinant instead of PBE like the results in Figure 4, it is apparent that even in cases where $\langle\hat{S}^2\rangle$ does not increase upon annihilation of the $(S+1)$ state, it is still possible that the $(S+2)$ state can play a large role. The use of DFT generally reduces the effect of spin contamination and so will decrease the importance of annihilating $(S+2)$ and higher states. However, the findings illustrated by Figure 4 and Table 3 imply that improved performance of Δ-Proj-DH-DFT requires use of a more general projector that can recouple arbitrary numbers of symmetry broken electron spin pairs.

Rydberg Excitations. Rydberg excitations are known to be challenging for TDDFT owing to the diffuse nature of the virtual orbitals which accept an electron and are not properly described due to the incorrect asymptotic behavior of the exchange−correlation contribution to the density.[67] Use of exact HF exchange has been found to significantly improve the prediction of VEEs in TDDFT calculations, although there has been little investigation of difference approaches for studying Rydberg states. Figure 5 shows the performance of the four difference methods in describing VEE to Rydberg states. Examining the mean error with respect to HF exchange in Figure 5, it can be seen that Rydberg states show a different

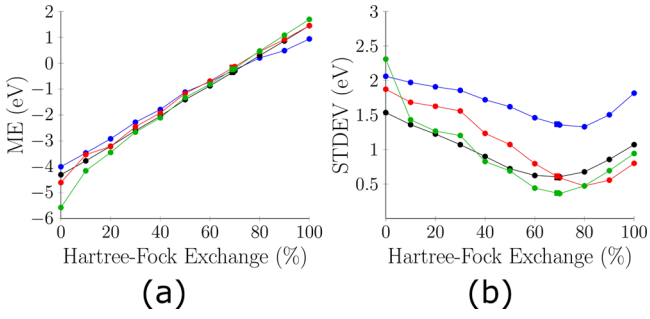

Figure 5. Mean error (a) and standard deviation (b) of Rydberg vertical excitation energies as a function of Hartree−Fock exchange percentage for ΔPAV-DH-DFT (red), ΔDH-DFT (green), ΔPAV-DFT (blue), and ΔDFT (black) compared to benchmark values, without data in which $\langle\hat{S}^2\rangle$ of the reference increases upon projection. Squares show the results at 69% Hartree−Fock exchange.

https://doi.org/10.1021/acs.jpca.2c04338
J. Phys. Chem. A XXXX, XXX, XXX−XXX

trend to local and charge transfer excitations, with little difference between projected and unprojected functionals, or between hybrid and double-hybrid functionals, and a linear correlation between VEE and HF exchange. As a result, all functionals cross the zero mean error line between 70% and 80% HF exchange, with the MP2 corrected functionals crossing at slightly lower values (72.2% for Δ-Proj-DH-DFT and 72.9% for ΔDH-DFT) than the hybrid functionals (75.5% for Δ-Proj-DFT and 75.0% for ΔDFT). Due to the similar performance of all functionals in terms of mean error, the best performing functional for computing Rydberg excitations can be selected using the lowest standard deviation at the point that the mean error crosses zero (Figure 5b). The performance of Δ-Proj-DFT is poor at all amount of HF exchange, while Δ-Proj-DH-DFT only performs well at high HF exchange. MP2 correlation significantly improves the standard deviation of projected functionals, while unprojected functionals only give a noticeable difference in performance above 60% exact exchange. The best standard deviation is achieved at 70% exact exchange for unprojected methods and at 80% exact exchange for projected methods. However, even though above 80% exact exchange, Δ-Proj-DH-DFT gives the best results, which is the opposite behavior to charge transfer and local excitations, and increasing HF exchange causes the performance of all functionals to diminish.

Overall Performance. The performance for all three excitation types in the Tozer benchmark is shown in Figure 6. The trend in mean error reflects that of local and charge transfer excitations, with projection giving better performance at low HF exchange, while the use of perturbation theory improves the result at high HF exchange. At 60−70% HF exchange, the crossover between the two effects leads to a very similar mean error in all four methods tested. Increasing the HF exchange to around 80% in unprojected double-hybrid density functional theory will lead to the lowest mean error, and the unprojected double-hybrid is the only method that crosses the zero mean error axis. The mean error for the projected double-hybrid functional is also minimized at 80% HF exchange. For unprojected hybrid functionals, the best HF exchange parameter is 100%, although this value is a consequence of error cancellation where Rydberg excitations overestimate the VEE, while local and charge transfer excitations underestimate the VEE. Projected hybrid functionals are the best choice for low HF exchange, particularly at the 15−30% range of many common hybrid functionals.

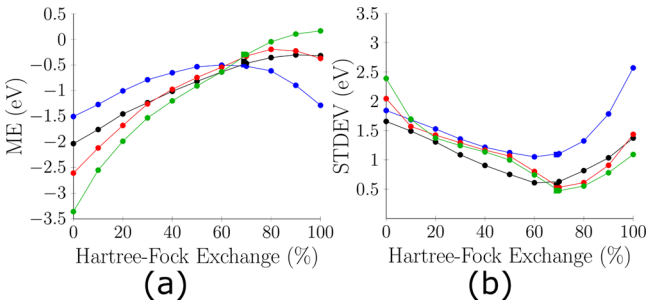

Figure 6. Mean error (a) and standard deviation (b) of all classes of vertical excitation energies as a function of Hartree−Fock exchange percentage for ΔPAV-DH-DFT (red), ΔDH-DFT (green), ΔPAV-DFT (blue), and ΔDFT (black) compared to benchmark values. Squares show the results at 69% Hartree−Fock exchange.

However, even projected hybrid functionals would benefit from a larger amount HF exchange, around 60%, in order to minimize error in the calculation of Rydberg VEEs.

Although it is possible to tune all four functionals to obtain mean errors of −0.5 eV below the benchmark value, the standard deviation gives good reason to use double-hybrid functionals over hybrid functionals. Figure 6b shows that the minimum standard deviation for double-hybrid functionals is at 70% HF exchange, while for hybrid functionals, the lowest standard deviation is at 60%. However, for unprojected hybrid functionals, the lowest mean error is at 100%, where all four functionals show increased standard deviation. For the projected hybrid functional, even though the lowest mean error and standard deviation coincide at the same HF exchange, the standard deviation is twice as large as for all three other methods. The double-hybrid functionals give similar mean error and standard deviation at both 70% and 80% HF exchange, indicating the advantage of double hybrid functionals in providing low mean error and standard deviation at the same value of HF exchange. For ΔDH-DFT, the performance limit is a mean error of 0 eV with a standard deviation of 0.5 eV. While projection gives better performance for local excitations, the failures for charge transfer states at high HF exchange mean that overall it does not improve the performance. However, as the failure of projection appears to be a result of multiple contaminating states at high HF exchange which cannot be accounted for with the Löwdin annihilator, development of alternative projection formalisms may further improve the performance and yield better results than the unprojected approach across all excitation types.

The failure of the Löwdin projector at high amount of exact exchange can be emphasized by examination of the average $\langle \hat{S}^2 \rangle$ for the excited state calculation. With the standard parametrization (69%) where Δ-Proj-DH-DFT performs best, the average $\langle \hat{S}^2 \rangle$ is 1.04 for local excited states, 1.07 for charge transfer states, and 1.02 for Rydberg states. These results indicate that regardless of the character of the excited state, all excitations could be characterized as breaking a single electron pair where the Löwdin projector should work well, with very little spin polarization of the remaining $N - 2$ electrons in response to the excitation. Increasing the exact exchange to 100% gives average $\langle \hat{S}^2 \rangle$ of 1.18 for local excitations, 1.22 for charge transfer, and 1.08 for Rydberg states. As a result, it is apparent that higher amounts of exact exchange lead to greater spin contamination, although it appears that Rydberg states are less affected, suggesting that local and charge transfer states are most likely to lead to failure of the Löwdin projector.

CONCLUSIONS

In this work we performed the first systematic investigation of the performance of difference approaches for studying different types of electronic excitations (local, charger transfer, and Rydberg). In particular, we examined how hybrid and double-hybrid functionals performed, along with the importance of including projection to account for strong correlation from breaking an electron pair in the excitation. Furthermore, given the known importance of using exact HF exchange for properly describing charge transfer and Rydberg excitations, we examined the role of the HF exchange parameter on controlling the mean error and standard deviation. Overall, the local excitation VEEs corroborated the findings from our

https://doi.org/10.1021/acs.jpca.2c04338
J. Phys. Chem. A XXXX, XXX, XXX−XXX

previous study using a different test set, which demonstrated that projected double-hybrid functionals give the smallest standard deviation. However, in the previous work, the default HF exchange of the double-hybrid functional was used for all functionals tested. As a result, the poor performance of hybrid functionals may have been a reflection of the poor parametrization used.

We identified that for local excitations, projected hybrid functionals provide a similar performance to projected double-hybrid functionals and the HF exchange parameter is parametrized differently (70% for double hybrids and 20% for hybrids). For charge-transfer and Rydberg VEEs, hybrid functionals with 20% HF exchange show worse performance compared to double-hybrid functionals with larger amounts of HF exchange. Increasing HF exchange for projected hybrid functionals can give better mean errors and standard deviation, although the standard deviation is higher than double-hybrid functionals, especially for Rydberg excitations. As a result, while projected hybrid functionals with around 20% are suitable for local excitations and reasonable performance can be obtained with around 60% HF exchange for Rydberg and charge transfer states, only double-hybrid functionals provide good performance in terms of precision and accuracy across all three excitation types for a fixed amount of HF exchange (between 70% and 80%).

When examining how different terms in the functional change the performance as a function of HF exchange, two clear trends were observed. First, at low amounts of HF exchange, MP2 correlation significantly degrades the performance of local and charge transfer VEEs. The poor double-hybrid performance with low amounts of exact exchange is a result of double counting of strong correlation, as the low amount of exact exchange implies a high amount of DFT exchange, which accounts for static correlation through inclusion of an exchange hole. In addition, low HF exchange contribution reduces the frontier orbital energy gap causing numerical issues in the correlation term, which may be partially fixed by regularization. Second, projection degrades the performance of functionals at high amounts of HF exchange due to the increased contributions of higher-order contaminating spin states which the Löwdin projector is unable to account for. Implementation of the method using alternative forms of the projector that can recouple arbitrary numbers of electron pairs may improve the performance and extend the applicability of the model to multielectron excitations and open-shell ground states. Future work should also involve developing transition dipole moments to enable spectral simulation, and work in the group is currently progressing in this direction.

■ ASSOCIATED CONTENT

Supporting Information

The Supporting Information is available free of charge at https://pubs.acs.org/doi/10.1021/acs.jpca.2c04338.

VEEs and $\langle \hat{S}^2 \rangle$ values for all computed states, mean error, and standard deviation for different values of a_x broken down by excitation type, additional graphs plotting the mean error and standard deviation discounting data points with anomalous $\langle \hat{S}^2 \rangle$ behavior upon projection, and additional graphs plotting the correlation between HOMO−LUMO energy gap and mean error for different amounts of exact exchange by excitation type (PDF)

■ AUTHOR INFORMATION

Corresponding Author

Lee M. Thompson − *Department of Chemistry, University of Louisville, Louisville, Kentucky 40205, United States;* orcid.org/0000-0003-1485-5934; Email: lee.thompson.1@louisville.edu

Authors

Emily M. Kempfer-Robertson − *Department of Chemistry, University of Louisville, Louisville, Kentucky 40205, United States*

Meagan N. Haase − *Department of Chemistry, University of Louisville, Louisville, Kentucky 40205, United States*

Jonathan S. Bersson − *Department of Chemistry, University of Louisville, Louisville, Kentucky 40205, United States*

Irma Avdic − *Department of Chemistry, University of Louisville, Louisville, Kentucky 40205, United States*

Complete contact information is available at: https://pubs.acs.org/10.1021/acs.jpca.2c04338

Notes

The authors declare no competing financial interest.

■ ACKNOWLEDGMENTS

This material is based upon work supported by the National Science Foundation under Grant 2144905. E.M.K.-R. acknowledges funding through the Arno Spatola Endowment Fellowship. This work was conducted in part using the resources of the University of Louisville's research computing group and the Cardinal Research Cluster.

■ REFERENCES

(1) Cheng, Y.-C.; Fleming, G. R. Dynamics of light harvesting in photosynthesis. *Annu. Rev. Phys. Chem.* **2009**, *60*, 241−262.

(2) Evrard, C. N.; Mahler, A. D.; Thompson, L. M. In *Computational Photocatalysis: Modeling of Photophysics and Photochemistry at Interfaces*; Han, Y., Kilin, D. S., Kilina, S., Eds.; ACS Symposium Series, Vol. 1331; American Chemical Society, 2019; Chapter 15, pp 327−341.

(3) Neugebauer, J. Subsystem-based theoretical spectroscopy of biomolecules and biomolecular assemblies. *ChemPhysChem* **2009**, *10*, 3148−3173.

(4) Thompson, L. M.; Lasoroski, A.; Champion, P. M.; Sage, J. T.; Frisch, M. J.; van Thor, J. J.; Bearpark, M. J. Analytical harmonic vibrational frequencies for the green fluorescent protein computed with ONIOM: Chromophore mode character and its response to environment. *J. Chem. Theory Comput.* **2014**, *10*, 751−766.

(5) Coropceanu, V.; Chen, X.-K.; Wang, T.; Zheng, Z.; Brédas, J.-L. Charge-transfer electronic states in organic solar cells. *Nat. Rev. Mater.* **2019**, *4*, 689−707.

(6) Khan, S. U. Z.; Londi, G.; Liu, X.; Fusella, M. A.; D'Avino, G.; Muccioli, L.; Brigeman, A. N.; Niesen, B.; Yang, T. C. J.; Olivier, Y.; et al. Multiple charge transfer states in donor-acceptor heterojunctions with large frontier orbital energy offsets. *Chem. Mater.* **2019**, *31*, 6808−6817.

(7) Cornil, J.; Verlaak, S.; Martinelli, N.; Mityashin, A.; Olivier, Y.; Van Regemorter, T.; D'Avino, G.; Muccioli, L.; Zannoni, C.; Castet, F.; et al. Exploring the energy landscape of the charge transport levels in organic semiconductors at the molecular scale. *Acc. Chem. Res.* **2013**, *46*, 434−443.

(8) Tozer, D. J.; Handy, N. C. On the determination of excitation energies using density functional theory. *Phys. Chem. Chem. Phys.* **2000**, *2*, 2117−2121.
(9) Mardirossian, N.; Head-Gordon, M. ωb97X-V: A 10-parameter, range-separated hybrid, generalized gradient approximation density functional with nonlocal correlation, designed by a survival-of-the-fittest strategy. *Phys. Chem. Chem. Phys.* **2014**, *16*, 9904−9924.
(10) Dreuw, A.; Head-Gordon, M. Failure of time-dependent density functional theory for long-range charge-transfer excited states: The zincbacteriochlorin bacteriochlorin and bacteriochlorophyll spheroidene complexes. *J. Am. Chem. Soc.* **2004**, *126*, 4007−4016.
(11) Kümmel, S. Charge-transfer excitations: A challenge for time-dependent density functional theory that has been met. *Adv. Energy Mater.* **2017**, *7*, 1700440.
(12) Maitra, N. T. Charge transfer in time-dependent density functional theory. *J. Phys.: Condens. Matter* **2017**, *29*, 423001.
(13) Hait, D.; Rettig, A.; Head-Gordon, M. Well-behaved versus ill-behaved density functionals for single bond dissociation: Separating success from disaster functional by functional for stretched H2. *J. Chem. Phys.* **2019**, *150*, 094115.
(14) Rohrdanz, M. A.; Martins, K. M.; Herbert, J. M. A long-range-corrected density functional that performs well for both ground-state properties and time-dependent density functional theory excitation energies, including charge-transfer excited states. *J. Chem. Phys.* **2009**, *130*, 054112.
(15) Mendes, R. A.; Haiduke, R. L. A.; Bartlett, R. J. The devil's triangle of Kohn-Sham density functional theory and excited states. *J. Chem. Phys.* **2021**, *154*, 074106.
(16) Nam, S.; Cho, E.; Sim, E.; Burke, K. Explaining and fixing DFT failures for torsional barriers. *J. Phys. Chem. Lett.* **2021**, *12*, 2796−2804.
(17) Athavale, V.; Teh, H.-H.; Subotnik, J. E. On the inclusion of one double within CIS and TDDFT. *J. Chem. Phys.* **2021**, *155*, 154105.
(18) Grimme, S.; Neese, F. Double-hybrid density functional theory for excited electronic states of molecules. *J. Chem. Phys.* **2007**, *127*, 154116.
(19) Grimme, S.; Neese, F. Double-hybrid density functional theory for excited electronic states of molecules. *J. Chem. Phys.* **2007**, *127*, 154116.
(20) Goerigk, L.; Moellmann, J.; Grimme, S. Computation of accurate excitation energies for large organic molecules with double-hybrid density functionals. *Phys. Chem. Chem. Phys.* **2009**, *11*, 4611−12.
(21) Rubio, A.; Marques, M. Time-dependent density-functional theory. *Phys. Chem. Chem. Phys.* **2009**, *11*, 4436−4436.
(22) Meo, F. D.; Trouillas, P.; Adamo, C.; Sancho-García, J. C. Application of recent double-hybrid density functionals to low-lying singlet-singlet excitation energies of large organic compounds. *J. Chem. Phys.* **2013**, *139*, 164104.
(23) Brémond, E.; Sancho-García, J. C.; Pérez-Jiménez, A. J.; Adamo, C. Communication: Double-hybrid functionals from adiabatic-connection: The QIDH model. *J. Chem. Phys.* **2014**, *141*, 031101.
(24) Stanton, J. F.; Bartlett, R. J. The equation of motion coupled-cluster method. A systematic biorthogonal approach to molecular excitation energies, transition probabilities, and excited state properties. *J. Chem. Phys.* **1993**, *98*, 7029−7039.
(25) Christiansen, O.; Koch, H.; Jørgensen, P. The second-order approximate coupled cluster singles and doubles model CC2. *Chem. Phys. Lett.* **1995**, *243*, 409−418.
(26) Mehta, N.; Casanova-Páez, M.; Goerigk, L. Semi-empirical or non-empirical double-hybrid density functionals: which are more robust? *Phys. Chem. Chem. Phys.* **2018**, *20*, 23175−23194.
(27) Kempfer-Robertson, E. M.; Pike, T. D.; Thompson, L. M. Difference projection-after-variation double-hybrid density functional theory applied to the calculation of vertical excitation energies. *J. Chem. Phys.* **2020**, *153*, 074103.
(28) Goerigk, L.; Moellmann, J.; Grimme, S. Computation of accurate excitation energies for large organic molecules with double-hybrid density functionals. *Phys. Chem. Chem. Phys.* **2009**, *11*, 4611−4620.
(29) Schwabe, T.; Goerigk, L. Time-Dependent double-hybrid density functionals with spin-component and spin-opposite scaling. *J. Chem. Theory Comput.* **2017**, *13*, 4307−4323.
(30) Goerigk, L.; Grimme, S. Calculation of electronic circular dichroism spectra with time-dependent double-hybrid density functional theory. *J. Phys. Chem. A* **2009**, *113*, 767−776.
(31) Goerigk, L.; Grimme, S. Double-hybrid density functionals provide a balanced description of excited $1L_a$ and $1L_b$ states in polycyclic aromatic hydrocarbons. *J. Chem. Theory Comput* **2011**, *7*, 3272−3277.
(32) Goerigk, L.; Grimme, S. Assessment of TD-DFT methods and of various spin scaled CIS(D) and CC2 versions for the treatment of low-lying valence excitations of large organic dyes. *J. Chem. Phys.* **2010**, *132*, 184103.
(33) Ottochian, A.; Morgillo, C.; Ciofini, I.; Frisch, M. J.; Scalmani, G.; Adamo, C. Double hybrids and time-dependent density functional theory: An implementation and benchmark on charge transfer excited states. *J. Comput. Chem.* **2020**, *41*, 1242−1251.
(34) Casanova-Páez, M.; Goerigk, L. Global double hybrids do not work for charge transfer: A comment on "Double hybrids and time-dependent density functional theory: An implementation and benchmark on charge transfer excited states". *J. Comput. Chem.* **2021**, *42*, 528−533.
(35) Brémond, É.; Ottochian, A.; Pérez-Jiménez, Á. J.; Ciofini, I.; Scalmani, G.; Frisch, M. J.; Sancho-García, J. C.; Adamo, C. Assessing challenging intra-and inter-molecular charge-transfer excitations energies with double-hybrid density functionals. *J. Comput. Chem.* **2021**, *42*, 970−981.
(36) Mester, D.; Kállay, M. A simple range separated double-hybrid density functional theory for excited states. *J. Chem. Theory Comput.* **2021**, *17*, 927−942.
(37) Casanova-Páez, M.; Goerigk, L. Assessing the Tamm-Dancoff approximation, singlet-singlet, and singlet-triplet excitations with the latest long-range corrected double-hybrid density functionals. *J. Chem. Phys.* **2020**, *153*, 064106.
(38) Casanova-Páez, M.; Dardis, M. B.; Goerigk, L. ωB2PLYP and ωB2GPPLYP: The first two double-hybrid density functionals with long-range correction optimized for excitation energies. *J. Chem. Theory Comput.* **2019**, *15*, 4735−4744.
(39) Goerigk, L.; Casanova-Paéz, M. The trip to the density functional theory zoo continues: Making a case for time-dependent double hybrids for excited-state problems. *Aust. J. Chem.* **2021**, *74*, 3.
(40) Brémond, E.; Pérez-Jiménez, A. J.; Sancho-García, J. C.; Adamo, C. Range-separated hybrid and double-hybrid density functionals: A quest for the determination of the range-separation parameter. *J. Chem. Phys.* **2020**, *152*, 244124.
(41) Wilbraham, L.; Adamo, C.; Ciofini, I. Communication: Evaluating non-empirical double hybrid functionals for spin-state energetics in transition-metal complexes. *J. Chem. Phys.* **2018**, *148*, 041103.
(42) Chen, W.; Schlegel, H. B. Evaluation of S2 for correlated wave functions and spin projection of unrestricted Møller-Plesset perturbation theory. *J. Chem. Phys.* **1994**, *101*, 5957−5968.
(43) Kitsaras, M.-P.; Stopkowicz, S. Spin contamination in MP2 and CC2, a surprising issue. *J. Chem. Phys.* **2021**, *154*, 131101.
(44) Knowles, P. J.; Handy, N. C. Convergence of projected unrestricted Hartee-Fock Møller-Plesset series. *J. Phys. Chem.* **1988**, *92*, 3097−3100.
(45) Handy, N. C.; Knowles, P. J. Projected unrestricted Møller−Plesset second-order energies. *J. Chem. Phys.* **1988**, *88*, 6991−6998.
(46) Lowdin, P.-O. Quantum theory of many-particle systems. III. Extension of the Hartree-Fock scheme to include degenerate systems and correlation effects. *Phys. Rev.* **1955**, *97*, 1509−1520.

https://doi.org/10.1021/acs.jpca.2c04338
J. Phys. Chem. A XXXX, XXX, XXX−XXX

(47) Scuseria, G. E.; Jiménez-Hoyos, C. A.; Henderson, T. M.; Samanta, K.; Ellis, J. K. Projected quasiparticle theory for molecular electronic structure. *J. Chem. Phys.* **2011**, *135*, 124108.
(48) Jiménez-Hoyos, C. A.; Henderson, T. M.; Tsuchimochi, T.; Scuseria, G. Projected Hartree-Fock theory. *J. Chem. Phys.* **2012**, *136*, 164109.
(49) Tóth, Z.; Pulay, P. Finding symmetry breaking Hartree-Fock solutions: The case of triplet instability. *J. Chem. Phys.* **2016**, *145*, 164102.
(50) Mahler, A. D.; Thompson, L. M. Orbital optimization in nonorthogonal multiconfigurational self-consistent field applied to the study of conical intersections and avoided crossings. *J. Chem. Phys.* **2021**, *154*, 244101.
(51) Lee, J.; Head-Gordon, M. Regularized Orbital-Optimized Second-Order Møller−Plesset Perturbation Theory: A Reliable Fifth-Order-Scaling Electron Correlation Model with Orbital Energy Dependent Regularizers. *J. Chem. Theory Comput.* **2018**, *14*, 5203−5219.
(52) Peach, M. J. G.; Benfield, P.; Helgaker, T.; Tozer, D. J. Excitation energies in density functional theory: An evaluation and a diagnostic test. *J. Chem. Phys.* **2008**, *128*, 044118.
(53) Grimme, S. Improved second-order Möller-Plesset perturbation theory by separate scaling of parallel- and antiparallel-spin pair correlation energies. *J. Chem. Phys.* **2003**, *118*, 9095−9102.
(54) Kozuch, S.; Martin, J. M. L. DSD-PBEP86: in search of the best double-hybrid DFT with spin-component scaled MP2 and dispersion corrections. *Phys. Chem. Chem. Phys.* **2011**, *13*, 20104−20107.
(55) Kozuch, S.; Martin, J. M. Spin-component-scaled double hybrids: an extensive search for the best fifth-rung functionals blending DFT and perturbation theory. *J. Comput. Chem.* **2013**, *34*, 2327−2344.
(56) Gilbert, A. T. B.; Besley, N. A.; Gill, P. M. W. Self-consistent field calculations of excited states using the maximum overlap method (MOM). *J. Phys. Chem. A* **2008**, *112*, 13164−13171.
(57) Barca, G. M. J.; Gilbert, A. T. B.; Gill, P. M. W. Simple models for difficult electronic excitations. *J. Chem. Theory Comput.* **2018**, *14*, 1501−1509.
(58) Carter-Fenk, K.; Herbert, J. M. State-targeted energy projection: A simple and robust approach to orbital relaxation of non-Aufbau self-consistent field solutions. *J. Chem. Theory Comput* **2020**, *16*, 5067−5082.
(59) Frisch, M. J.; Trucks, G. W.; Schlegel, H. B.; Scuseria, G. E.; Robb, M. A.; Cheeseman, J. R.; Scalmani, G.; Barone, V.; Petersson, G. A.; Nakatsuji, H.; et al.*Gaussian 16*, revision A.03; Gaussian Inc.: Wallingford, CT, 2016.
(60) Neese, F. The ORCA program system. *Wiley Interdiscip. Rev.: Comput. Mol. Sci.* **2012**, *2*, 73−78.
(61) Thompson, L. M.; Sheng, X.; Mahler, A.; Mullally, D.; Hratchian, H. P.*MQCPack 22.6*; 2022; DOI: 10.5281/zenodo.6644196.
(62) Schreiber, M.; Silva-Junior, M. R.; Sauer, S. P. A.; Thiel, W. Benchmarks for electronically excited states: CASPT2, CC2, CCSD, and CC3. *J. Chem. Phys.* **2008**, *128*, 134110.
(63) Grimme, S. Semiempirical hybrid density functional with perturbative second-order correlation. *J. Chem. Phys.* **2006**, *124*, 034108.
(64) Baerends, E. J. Density functional approximations for orbital energies and total energies of molecules and solids. *J. Chem. Phys.* **2018**, *149*, 054105.
(65) Santra, G.; Martin, J. M. L. Do double-hybrid functionals benefit from regularization in the PT2 term? Observations from an extensive benchmark. *J. Phys. Chem. Lett.* **2022**, *13*, 3499−3506.
(66) Thompson, L. M.; Hratchian, H. P. On approximate projection models. *Mol. Phys.* **2019**, *117*, 1421−1429.
(67) Casida, M. E.; Jamorski, C.; Casida, K. C.; Salahub, D. R. Molecular excitation energies to high-lying bound states from time-dependent density-functional response theory: Characterization and correction of the time-dependent local density approximation ionization threshold. *J. Chem. Phys.* **1998**, *108*, 4439−4449.

https://doi.org/10.1021/acs.jpca.2c04338
J. Phys. Chem. A XXXX, XXX, XXX−XXX